

Ground-state and finite-temperature signatures of quantum phase transitions in the half-filled Hubbard model on a honeycomb lattice

Thereza Paiva,¹ R. T. Scalettar,² W. Zheng,³ R. R. P. Singh,² and J. Oitmaa³

¹*Instituto de Física, Universidade Federal do Rio de Janeiro, Caixa Postal 68.528, 21945-970 Rio de Janeiro, RJ, Brazil*

²*Physics Department, University of California, Davis, California 95616, USA*

³*School of Physics, University of New South Wales, Sydney NSW 2052, Australia*

(Received 22 June 2004; revised manuscript received 28 June 2005; published 17 August 2005)

We investigate ground state and finite temperature properties of the half-filled Hubbard model on a honeycomb lattice using quantum Monte Carlo and series expansion techniques. Unlike the square lattice, for which magnetic order exists at $T=0$ for any nonzero U , the honeycomb lattice is known to have a semimetal phase at small U and an antiferromagnetic one at large U . We investigate the phase transition at $T=0$ by studying the magnetic structure factor and compressibility using quantum Monte Carlo simulations and by calculating the sublattice magnetization, uniform susceptibility, spinwave, and single hole dispersion using series expansions around the ordered phase. Our results are consistent with a single continuous transition at U_c/t in the range 4–5. Finite-temperature signatures of this phase transition are seen in the behavior of the specific heat, $C(T)$, which changes from a two-peaked structure for $U > U_c$ to a one-peaked structure for $U < U_c$. Furthermore, the U dependence of the low temperature coefficient of $C(T)$ exhibits an anomaly at $U \approx U_c$.

DOI: [10.1103/PhysRevB.72.085123](https://doi.org/10.1103/PhysRevB.72.085123)

PACS number(s): 71.10.Fd, 75.10.Lp, 75.40.Mg

I. INTRODUCTION

The two-dimensional Hubbard-Hamiltonian has been extensively studied as a model of metal-insulator and magnetic phase transitions¹ and also within the context of systems such as the CuO_2 sheets of high temperature superconductors.² In the square-lattice case, at half-filling, nesting of the Fermi surface leads to a divergent antiferromagnetic susceptibility as the temperature is lowered, even for $U=0$, and thus the ground state is an antiferromagnetic insulator at any nonzero U . It is of interest to study cases where, instead, the transition to the antiferromagnetic phase occurs at finite U . In such a situation, for example, it may prove possible to see if the Mott metal-insulator and paramagnetic-antiferromagnetic phase transitions occur separately. A finite U_c also makes it more straightforward to study the thermodynamics at temperatures above the $T=0$ quantum phase transition, a question pertinent to experimental studies of such phase transitions.³

The two-dimensional honeycomb lattice is one geometry in which we can explore these issues. In this paper, we investigate the properties of the half-filled honeycomb lattice Hubbard model using determinant quantum Monte Carlo and series expansions methods. After a brief review of previous work, we describe the model and calculational approaches, and show data for a number of different ground state properties that carry signatures of the phase transition. Our overall results are consistent with a single continuous transition as a function of U/t . We then turn to the finite temperature behavior of the specific heat to see how such a critical point may be reflected in this key experimental property.

While the honeycomb lattice has U_c nonzero, it is important to note at the outset that, like the square lattice, its noninteracting density of states has a special feature. As shown in Fig. 1, $N(\omega)$ vanishes linearly as $\omega \rightarrow 0$, so the system is a semimetal (or alternatively, a zero-gap semiconductor) at

half filling. As a consequence, at weak coupling, the low temperature behavior of the specific heat is quadratic in temperature, $C = \delta T^2$, instead of the usual linear Fermi liquid dependence. At strong coupling, when long range antiferromagnetic order sets in, the specific heat will also be quadratic in T owing to the spin-wave excitations. How the specific heat evolves between these two regimes is an open question.

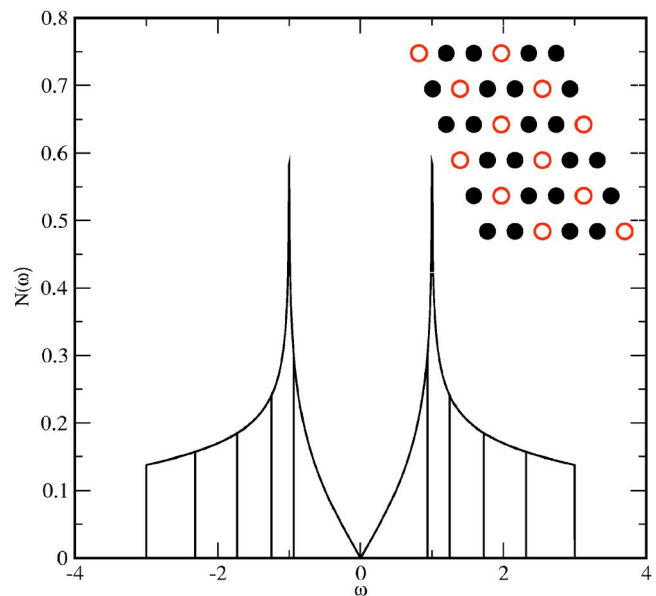


FIG. 1. (Color online) Noninteracting density of states of the Hubbard model on a honeycomb lattice. This geometry is bipartite, so $N(\omega)$ is symmetric about $\omega=0$. The vertical lines correspond to fillings of 0.1, 0.2, 0.3, etc. The density of states vanishes linearly at $\omega=0$ and has logarithmic Van Hove singularities at fillings $\rho=3/8$ and $5/8$. The bandwidth $W=6t$. Inset: honeycomb lattice (full symbols) and underlying triangular lattice (full and empty symbols), for $L=6$ and $N=24$.

A considerable body of work exists concerning the ground state phase diagram. Martelo *et al.* found that within mean field theory the Mott transition occurs below an upper bound for the critical interaction strength $U_c/t \approx 5.3$.⁴ Meanwhile, their variational Monte Carlo calculation suggested a lower bound for the antiferromagnetic transition $U_c/t \approx 3.7$. They interpreted these results as a single transition from paramagnetic metal to antiferromagnetic insulator at $U_c/t = 4.5 \pm 0.5$.

Sorella *et al.*⁵ and Furukawa⁶ studied the model using the random phase approximation which gives $U_c/t = 2.23$ for the onset of antiferromagnetic order. Auxiliary field quantum Monte Carlo (QMC) simulations⁵ using the ground state projection approach suggested $U_c/t = 4.5 \pm 0.5$. Projector QMC work by Furukawa⁶ on larger lattices and doing system size extrapolations resulted in a somewhat lower value, $U_c/t = 3.6 \pm 0.1$. Peres *et al.* have recently studied the phase diagram and mean field magnetization of coupled honeycomb layers as a function of filling, U/t , and interlayer hopping t'/t using the random phase approximation and spin wave analysis.⁷

In addition to antiferromagnetism and the Mott transition other phenomena associated with strong correlations have also been studied. As with the square lattice Hubbard model, Nagaoka ferromagnetism is also possible for the doped honeycomb lattice at strong couplings ($U/t > 12$) and was investigated by Hanisch *et al.* using Gutzwiller wave functions,⁸ and also by Peres *et al.*⁷ Renormalization group calculations by González *et al.*¹⁰ have addressed the non-Fermi liquid behavior of the half-filled honeycomb Hubbard model. As pointed by the authors, the existence of nontrivial scaling laws should show up in a variety of properties, including the specific heat.

We conclude this introduction by noting that the Hubbard model on a honeycomb lattice has also been suggested to be of interest for a variety of systems including graphite sheets,⁹ and carbon nanotubes,¹¹ as well as MgB₂ (Ref. 6) and Pb and Sn on Ge(111) surfaces.¹² The honeycomb lattice is also a 2/3 subset of the triangular lattice (see inset in Fig. 1), and so the nature of spin correlations on the honeycomb lattice has been considered as possibly relevant to the properties of triangular lattice systems like Na_xCoO₂ at appropriate dopings.¹³

II. HUBBARD HAMILTONIAN, DETERMINANT QUANTUM MONTE CARLO, AND SERIES EXPANSION METHODS

We study the Hubbard Hamiltonian,

$$H = -t \sum_{\langle \mathbf{i}, \mathbf{j} \rangle \sigma} (c_{\mathbf{i}\sigma}^\dagger c_{\mathbf{j}\sigma} + c_{\mathbf{j}\sigma}^\dagger c_{\mathbf{i}\sigma}) + U \sum_{\mathbf{i}} \left(n_{\mathbf{i}\uparrow} - \frac{1}{2} \right) \left(n_{\mathbf{i}\downarrow} - \frac{1}{2} \right) - \mu \sum_{\mathbf{i}} (n_{\mathbf{i}\uparrow} + n_{\mathbf{i}\downarrow}).$$

Here $c_{\mathbf{i}\sigma}^\dagger$ ($c_{\mathbf{i}\sigma}$) are creation (destruction) operators for a fermion of spin σ on lattice site \mathbf{i} . The kinetic energy term includes a sum over near neighbors $\langle \mathbf{i}, \mathbf{j} \rangle$ on a two-dimensional honeycomb lattice. We denote by N the number of lattice sites, and L the linear dimension of the lattice,

which corresponds to the linear dimension of the underlying triangular lattice, as shown in the inset to Fig. 1. The particular way the honeycomb lattice is cut out of the plane is a matter of taste. We have therefore $N = \frac{2}{3}L^2$ and we have used periodic boundary conditions. The interaction term is written in particle-hole symmetric form so that $\mu=0$ corresponds to half-filling: the density $\rho = \langle n_{\mathbf{i}\uparrow} + n_{\mathbf{i}\downarrow} \rangle = 1$ for all t, U , and temperatures T . We choose the hopping parameter $t=1$ to set the energy scale. Note that the noninteracting model has two Dirac points \mathbf{K}_\pm on the Fermi surface where the dispersion relation is relativistic,⁹ i.e., the energy grows linearly with $|\mathbf{k} - \mathbf{K}_\pm|$.

We use the determinant quantum Monte Carlo method to measure the properties of the Hamiltonian.^{14,15} In this approach the partition function is written as a path integral, the interaction term is decoupled through the introduction of a discrete auxiliary Hubbard–Stratonovich field,¹⁶ and the fermion degrees of freedom are traced out analytically. The remaining summation over the Hubbard–Stratonovich field is done stochastically. Since the lattice is bipartite, no sign problem occurs at half-filling. Data were typically generated by doing several tens of thousands of measurements at each data point (temperature, coupling constant, and lattice size). Global moves which flip the Hubbard–Stratonovich variables for all imaginary times at a given spatial site were included so that at stronger couplings, transitions between different densities are facilitated.¹⁷

We have also carried out an Ising type expansion for this system at $T=0$ using a linked-cluster method.¹⁸ Similar expansions were previously done for the Hubbard model on the square lattice.¹⁹ To perform the series expansion, one needs to introduce an Ising interaction into the Hubbard–Hamiltonian, and divide the Hamiltonian into an unperturbed Hamiltonian (H_0) and a perturbation (H_1) as follows:

$$H = H_0 + \lambda H_1$$

$$H_0 = J \sum_{\langle \mathbf{i}, \mathbf{j} \rangle} (\sigma_{\mathbf{i}}^z \sigma_{\mathbf{j}}^z + 1) + U \sum_{\mathbf{i}} \left(n_{\mathbf{i}\uparrow} - \frac{1}{2} \right) \left(n_{\mathbf{i}\downarrow} - \frac{1}{2} \right)$$

$$H_1 = \sum_{\langle \mathbf{i}, \mathbf{j} \rangle} [-J(\sigma_{\mathbf{i}}^z \sigma_{\mathbf{j}}^z + 1) - t(c_{\mathbf{i}\sigma}^\dagger c_{\mathbf{j}\sigma} + \text{H.c.})]$$

where $\sigma_{\mathbf{i}}^z = n_{\mathbf{i}\uparrow} - n_{\mathbf{i}\downarrow}$, and λ is the expansion parameter. Note that we are primarily interested in the behavior of the system at $\lambda=1$, at which point the Ising term cancels between H_0 and H_1 . The strength of the Ising interaction can be varied to improve convergence, and it proves useful to keep it of order t^2/U .¹⁹ The limits $\lambda=0$ and $\lambda=1$ correspond to the Ising model and the original model, respectively. This Hamiltonian will be called the Hubbard–Ising model. The unperturbed ground state is the usual Néel state. The Ising series have been calculated to order λ^{15} for the ground state energy, the staggered magnetization M , and the square of the local moment L_m ,¹⁹ and to order λ^{13} for the uniform magnetic susceptibility χ_\perp . The resulting power series in λ for $t/U=0.15$ and $J/U=0.0225$ are presented in Table I.

In addition to the ground state properties, we also compute the spin-wave dispersion Δ (to order λ^{13}) and the dis-

TABLE I. Series coefficients for Ising expansions of the ground-state energy per site, E_0/NU , the staggered magnetization M , squared local moment L_m , and the uniform magnetic susceptibility χ_\perp for $t/U=0.15$ and $J/U=0.0225$. Coefficients of λ^n up to order λ^{15} are listed.

n	E_0/NU	M	L_m	χ_\perp
0	-0.2501000000	1.0000000000	1.0000000000	3.703703704
1	0.0000000000	0.0000000000	0.0000000000	3.703703704
2	$-6.067415730 \times 10^{-2}$	$-1.090771367 \times 10^{-1}$	$-1.090771367 \times 10^{-1}$	-4.743810362
3	$-6.135588941 \times 10^{-3}$	$-2.206054451 \times 10^{-2}$	$-2.206054451 \times 10^{-2}$	-1.394196294×10^1
4	$-1.172455577 \times 10^{-2}$	$-3.552865175 \times 10^{-1}$	$-3.819372077 \times 10^{-2}$	-5.304439204
5	$-1.595132209 \times 10^{-2}$	$-7.348348039 \times 10^{-1}$	$-6.041765980 \times 10^{-2}$	2.402576623×10^1
6	$-2.167350013 \times 10^{-3}$	$-4.545288062 \times 10^{-1}$	$1.617075260 \times 10^{-2}$	3.836014584×10^1
7	$1.484188843 \times 10^{-2}$	$5.706090877 \times 10^{-1}$	$1.182931503 \times 10^{-1}$	-6.261816470
8	$1.982803975 \times 10^{-2}$	1.508870723	$1.282196638 \times 10^{-1}$	-8.556886959×10^1
9	$1.098873088 \times 10^{-2}$	1.362697325	$2.870390056 \times 10^{-2}$	-8.473956953×10^1
10	$-5.309942069 \times 10^{-3}$	$-9.038107499 \times 10^{-2}$	$-1.194968503 \times 10^{-1}$	7.394366538×10^1
11	$-2.087445585 \times 10^{-2}$	-1.988476084	$-2.381637820 \times 10^{-1}$	2.479347440×10^2
12	$-2.733805940 \times 10^{-2}$	-2.967041815	$-2.434002720 \times 10^{-1}$	1.283247884×10^2
13	$-1.868451700 \times 10^{-2}$	-2.220001906	$-7.558507985 \times 10^{-2}$	-3.404916769×10^2
14	$4.985233235 \times 10^{-3}$	$-1.210494842 \times 10^{-2}$	$2.437663805 \times 10^{-1}$	
15	$3.577717123 \times 10^{-2}$	2.934366446	$5.886265926 \times 10^{-1}$	

persion Δ_{1h} of one-hole added to half-filled system (to order λ^{11}). These calculations are possible by extending the similarity²⁰ and orthogonality transformation methods²¹ from Heisenberg and t - J models^{22,23} to the Hubbard–Ising models. The calculation of the dispersion involves a list of 28 811 clusters up to 13 sites. The series for the dispersions can be written in the following form:

$$\begin{aligned} \Delta(k_x, k_y) = & \sum_p \sum_{i,j} \frac{1}{3} a_{i,j,p} \lambda^p \{ \cos(ik_x/2) \cos(\sqrt{3}jk_y/2) \\ & + \cos[(i+3j)k_x/4] \cos[\sqrt{3}(i-j)k_y/4] \\ & + \cos[(i-3j)k_x/4] \cos[\sqrt{3}(i+j)k_y/4] \}. \end{aligned}$$

In Table II, we list the series coefficients $a_{i,j,p}$ for $t/U=0.15$ and $J/U=0.0225$. The series for other couplings are available from the authors upon request.

III. QUANTUM PHASE TRANSITION

We begin by examining the evidence for a phase transition in the model. First, we present results from the quantum Monte Carlo simulations, which can, in principle, address arbitrary t/U ratios.

A. Compressibility

The Mott metal–insulator transition is signaled by a vanishing compressibility $\kappa = \partial\rho/\partial\mu$. We show the difference between the density ρ and half-filling as a function of μ for $U/t=2$ and $U/t=7$ (Fig. 2). There is a clear qualitative difference in behavior. For weak coupling, ρ immediately shifts from half-filling as μ increases from zero, while at strong coupling, ρ remains pinned at $\rho=1$ out to finite μ . Although dealing with finite chemical potential the sign problem was

not severe for the temperatures, system sizes and strength of correlations considered.

In Fig. 3 we show how the density behaves with increasing β and L for $U/t=5$. The evolution with inverse temperature and lattice size suggests that there is a small, finite Mott gap at $U/t=5$. To analyze finite size effects we have plotted the density as a function of inverse system size L and extrapolated as $L \rightarrow \infty$, for a small chemical potential $\mu_0=0.2t$ as shown in the right panel of Fig. 4. The extrapolated densities as a function of U for $\beta=8$ and 10 are shown on the left panel of Fig. 4. We see that $\rho_0 \rightarrow 1$ at $U/t \approx 5$, signaling the onset of the Mott insulating phase.

B. Spin correlations and antiferromagnetic susceptibility

To study the magnetic behavior, we measure the real space spin correlations,

$$c_{zz}(\mathbf{r}) = \langle S_z(\mathbf{r}) S_z(\mathbf{0}) \rangle \quad S_z(\mathbf{r}) = n_{\mathbf{r}\uparrow} - n_{\mathbf{r}\downarrow}$$

$$c_{+-}(\mathbf{r}) = \langle S_-(\mathbf{r}) S_+(\mathbf{0}) \rangle \quad S_+(\mathbf{r}) = c_{\mathbf{r}\uparrow}^\dagger c_{\mathbf{r}\downarrow},$$

and their Fourier transforms,

$$S_{zz}(\mathbf{q}) = \sum_{\mathbf{r}} e^{i\mathbf{q}\cdot\mathbf{r}} c_{zz}(\mathbf{r})$$

$$S_{+-}(\mathbf{q}) = \sum_{\mathbf{r}} e^{i\mathbf{q}\cdot\mathbf{r}} c_{+-}(\mathbf{r}).$$

The quantities

$$c(\mathbf{r}) = c_{zz}(\mathbf{r}) + \frac{1}{2}[c_{+-}(\mathbf{r}) + c_{-+}(\mathbf{r})]$$

TABLE II. Series coefficients for the spin-wave excitation spectrum $\Delta(k_x, k_y)/U$ and one-hole dispersion $\Delta_{1h}(k_x, k_y)/U$. Nonzero coefficients up to order λ^{13} for $t/U=0.15$ and $J/U=0.0225$ are listed.

(p, i, j)	$a_{i,j,p}$	(p, i, j)	$a_{i,j,p}$	(p, i, j)	$a_{i,j,p}$	(p, i, j)	$a_{i,j,p}$
spin-wave excitation spectrum $\Delta(k_x, k_y)/U$							
(0, 0, 0)	$1.350000000 \times 10^{-1}$	(10, 0, 0)	$2.216091139 \times 10^{-1}$	(10, 3, 1)	$4.746162497 \times 10^{-1}$	(8, 6, 0)	$-7.225113429 \times 10^{-3}$
(1, 0, 0)	$-1.350000000 \times 10^{-1}$	(11, 0, 0)	$-1.393969235 \times 10^{-2}$	(11, 3, 1)	$-1.099204748 \times 10^{-1}$	(9, 6, 0)	$-2.262498583 \times 10^{-2}$
(2, 0, 0)	$1.111175434 \times 10^{-1}$	(12, 0, 0)	$-5.637616v584 \times 10^{-1}$	(12, 3, 1)	-1.440323067	(10, 6, 0)	$-2.696906952 \times 10^{-2}$
(3, 0, 0)	$2.082046617 \times 10^{-2}$	(13, 0, 0)	-1.304334460	(13, 3, 1)	-3.353557841	(11, 6, 0)	$6.591260743 \times 10^{-3}$
(4, 0, 0)	$-4.424242442 \times 10^{-2}$	(4, 3, 1)	$-1.237981890 \times 10^{-1}$	(8, 6, 2)	$-3.350958277 \times 10^{-3}$	(12, 6, 0)	$-2.916010244 \times 10^{-3}$
(5, 0, 0)	$-3.676674665 \times 10^{-2}$	(5, 3, 1)	$-1.341231436 \times 10^{-1}$	(9, 6, 2)	$-1.098231382 \times 10^{-2}$	(13, 6, 0)	$-2.568183304 \times 10^{-1}$
(6, 0, 0)	$-9.749111612 \times 10^{-3}$	(6, 3, 1)	$-2.171649093 \times 10^{-2}$	(10, 6, 2)	$-1.153863507 \times 10^{-2}$	(12, 9, 3)	$-1.609104960 \times 10^{-3}$
(7, 0, 0)	$2.153747460 \times 10^{-2}$	(7, 3, 1)	$1.086787464 \times 10^{-1}$	(11, 6, 2)	$7.460180712 \times 10^{-3}$	(13, 9, 3)	$-8.451196579 \times 10^{-3}$
(8, 0, 0)	$9.813204715 \times 10^{-2}$	(8, 3, 1)	$2.930587649 \times 10^{-1}$	(12, 6, 2)	$7.410248941 \times 10^{-3}$	(12, 9, 1)	$-9.742145152 \times 10^{-3}$
(9, 0, 0)	$2.080499557 \times 10^{-1}$	(9, 3, 1)	$5.034160236 \times 10^{-1}$	(13, 6, 2)	$-1.092694552 \times 10^{-1}$	(13, 9, 1)	$-5.101138671 \times 10^{-2}$
one-hole dispersion $\Delta_{1h}(k_x, k_y)/U$							
(0, 0, 0)	$5.675000000 \times 10^{-1}$	(7, 3, 1)	5.141564645	(8, 6, 0)	-1.091561629	(9,12, 4)	$-2.562349516 \times 10^{-6}$
(1, 0, 0)	$-6.750000000 \times 10^{-2}$	(8, 3, 1)	-1.258196166×10^1	(9, 6, 0)	-5.455143302	(10,12, 4)	$2.676464885 \times 10^{-3}$
(2, 0, 0)	$-6.336614782 \times 10^{-1}$	(9, 3, 1)	-1.733463014×10^2	(10, 6, 0)	5.327561412	(11,12, 4)	$1.433265640 \times 10^{-2}$
(3, 0, 0)	$-7.336392902 \times 10^{-1}$	(10, 3, 1)	-6.526403290×10^1	(11, 6, 0)	8.443452858×10^1	(8,12, 2)	$-2.978280918 \times 10^{-5}$
(4, 0, 0)	2.938067768	(11, 3, 1)	3.901815114×10^3	(6, 9, 3)	$8.189533379 \times 10^{-5}$	(9,12, 2)	$-2.049879613 \times 10^{-5}$
(5, 0, 0)	1.013199055×10^1	(4, 6, 2)	$-2.251112570 \times 10^{-3}$	(7, 9, 3)	$3.983472192 \times 10^{-5}$	(10,12, 2)	$2.139465782 \times 10^{-2}$
(6, 0, 0)	-1.702110647×10^1	(5, 6, 2)	$-6.420330616 \times 10^{-4}$	(8, 9, 3)	$1.025604453 \times 10^{-2}$	(11,12, 2)	$1.146460686 \times 10^{-1}$
(7, 0, 0)	-1.514268463×10^2	(6, 6, 2)	$2.127063569 \times 10^{-2}$	(9, 9, 3)	$4.129584046 \times 10^{-2}$	(8,12, 0)	$-2.233710688 \times 10^{-5}$
(8, 0, 0)	-4.655833834	(7, 6, 2)	$6.346958017 \times 10^{-2}$	(10, 9, 3)	$-2.110091800 \times 10^{-1}$	(9,12, 0)	$-1.537409710 \times 10^{-5}$
(9, 0, 0)	2.217144323×10^3	(8, 6, 2)	$-5.148299650 \times 10^{-1}$	(11, 9, 3)	-1.677872051	(10,12, 0)	$1.604362363 \times 10^{-2}$
(10, 0, 0)	3.740789745×10^3	(9, 6, 2)	-2.603465931	(6, 9, 1)	$4.913720027 \times 10^{-4}$	(11,12, 0)	$8.598244287 \times 10^{-2}$
(11, 0, 0)	-2.947388888×10^4	(10, 6, 2)	2.034643910	(7, 9, 1)	$2.390083315 \times 10^{-4}$	(10,15, 5)	$1.895585905 \times 10^{-7}$
(2, 3, 1)	$1.238532110 \times 10^{-1}$	(11, 6, 2)	3.720022590×10^1	(8, 9, 1)	$6.168519384 \times 10^{-2}$	(11,15, 5)	$1.687061931 \times 10^{-7}$
(3, 3, 1)	$1.022641192 \times 10^{-2}$	(4, 6, 0)	$-4.502225139 \times 10^{-3}$	(9, 9, 1)	$2.478775229 \times 10^{-1}$	(10,15, 3)	$1.895585905 \times 10^{-6}$
(4, 3, 1)	$7.872629131 \times 10^{-2}$	(5, 6, 0)	$-1.284066123 \times 10^{-3}$	(10, 9, 1)	-1.373111288	(11,15, 3)	$1.687061931 \times 10^{-6}$
(5, 3, 1)	$8.219599490 \times 10^{-3}$	(6, 6, 0)	$4.204959522 \times 10^{-2}$	(11, 9, 1)	-1.064077735×10^1	(10,15, 1)	$3.791171810 \times 10^{-6}$
(6, 3, 1)	$6.643492076 \times 10^{-1}$	(7, 6, 0)	$1.267005690 \times 10^{-1}$	(8,12, 4)	$-3.722851147 \times 10^{-6}$	(11,15, 1)	$3.374123863 \times 10^{-6}$

$$S(\mathbf{q}) = S_{zz}(\mathbf{q}) + \frac{1}{2}[S_{+-}(\mathbf{q}) + S_{-+}(\mathbf{q})]$$

average over the different spin orientation directions.

At $\beta \rightarrow \infty$ ($T=0$) and in the antiferromagnetically ordered phase at large U/t , the real space correlation will go asymptotically to a nonzero value $M^2/3$ at large separations \mathbf{r} , where M is the sublattice magnetization. In our finite temperature simulations, we access the $\beta \rightarrow \infty$ limit by cooling the system to the point where the correlation length exceeds the lattice size. In this case, the structure factor will grow linearly with lattice size N . More precisely, the structure factor will obey,

$$\frac{1}{N}S(\mathbf{q}) = \frac{M^2}{3} + \frac{a}{L},$$

where L is the linear lattice size.²⁴ In the paramagnetic phase at small U/t , the structure factor will be independent of N , and hence $S(\mathbf{q})/N$ vanish as $N \rightarrow \infty$.

In Fig. 5 we show $S(\pi, \pi)$ as a function of inverse temperature β for different lattice sizes at $U/t=7$ and the associated scaling plot. Also shown in Fig. 5 is the value of $c(\mathbf{r})$ for the largest separation on our finite lattices, $c(\mathbf{r}_{\max})$. This quantity should scale with the same intercept $M^2/3$ but a different finite size correction. We see that the system is in an antiferromagnetically ordered phase for this coupling.

Figure 6 shows analogous plots at $U/t=6$. The order parameter is still nonzero, but is quite small. Similar plots for $U/t=5$ are consistent with the vanishing of long range order. While we cannot pin down the location of the quantum phase transition exactly, a comparison of this analysis with the compressibility of Fig. 4 suggests that the vanishing of the compressibility gap and the antiferromagnetic order occur very close to each other and are in the neighborhood of $U_c/t \approx 5$.

C. Results from series expansions

We now present results from the Ising-type series expansions. These expansions are only valid in the magnetically

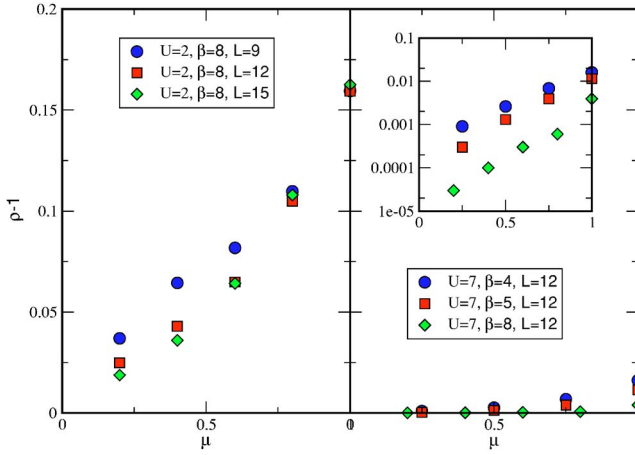


FIG. 2. (Color online) Difference in the value of the density ρ from half-filling as a function of chemical potential μ . At weak coupling ($U/t=2$, left panel) ρ is not pinned at one, but immediately begins to shift when $\mu \neq 0$: there is no Mott gap. At strong coupling ($U/t=7$, right panel), there is clear evidence for a Mott gap. As the logarithmic scale emphasizes (see inset), the densities at small positive μ are at least two orders of magnitude smaller than at weak coupling. Error bars (not shown) are smaller than data points.

ordered phase, and thus can only access the properties of the system for $U > U_c$.

In Fig. 7, we show the sublattice magnetization and uniform susceptibility. The QMC results for the sublattice magnetization are also shown. The two are roughly consistent with each other for small t/U . The uncertainties increase as the transition is approached. QMC results suggest a more abrupt drop to zero around $U/t \approx 5$, whereas the series results suggest a gradual decrease with increasing t/U . Since the series are not directly in the variable t/U but rather in an auxiliary variable λ , it is difficult to locate the true critical point U_c/t and obtain the critical properties. However, since we expect the critical exponent of the order parameter to be less than one, the true curve should come to zero with an

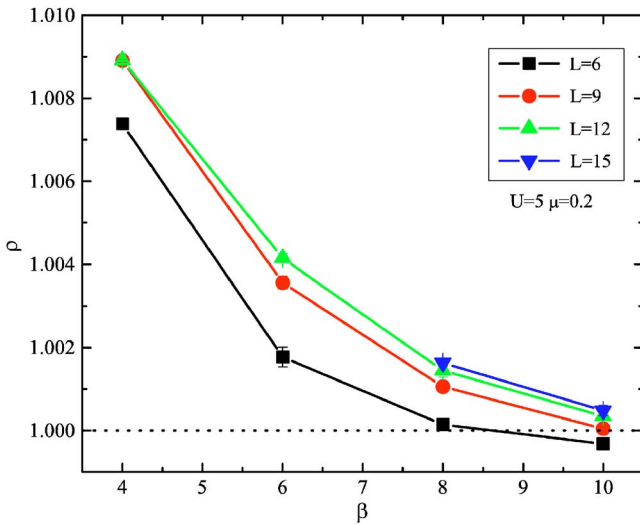


FIG. 3. (Color online) Density ρ at $\mu_0=0.2t$ as a function of the inverse temperature β for $U/t=5$ and different system sizes.

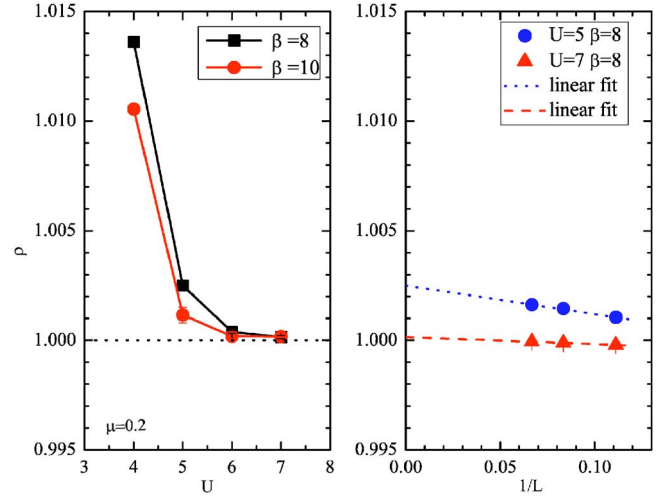


FIG. 4. (Color online) Right panel, ρ as a function of inverse linear size L , for $\mu=0.2t$, $\beta=8$, and $U/t=5$ and 7 . Left panel: extrapolated density ρ at $\mu_0=0.2t$ as a function of U .

infinite slope. Thus, from the series results alone, one would estimate $U_c/t \approx 4$, and this is in agreement with the estimate from the susceptibility χ_{\perp} also shown in Fig. 7.

Next, in Fig. 8, we show the spin-wave dispersion along high-symmetry cuts through the Brillouin zone for $t/U=0.1$, together with the dispersion obtained from first and second order spin-wave results for the Heisenberg model on a honeycomb lattice,²² which should approach the dispersion for the Hubbard model in the large U limit. As discussed previously, it is important to note that series expansions are developed for the Hubbard-Ising model, which starts with an unperturbed model with an anisotropy and a gap. The spin rotational symmetry is restored at $\lambda=1$, where the gap must close in the ordered phase. The limit $\lambda \rightarrow 1$ has power-law singularities in the series, which has to be treated by series extrapolation methods well known from the study of critical phenomena.²⁵ The numerical results obtained are consistent with gapless excitations in the Hubbard model. We can see that the dispersion has its minimum at the Γ point. The spin-wave dispersion for the Heisenberg model on a honeycomb lattice has a maximum at W point, while for the Hubbard model, this is only true for very small t/U . Already for $t/U=0.1$, the energy at W points is reduced, and the maximum moves to the K point.

Also, in Fig. 9 we show the one-hole dispersion for selected values of t/U . In principle, such a dispersion can be measured in angle resolved photoemission spectra (ARPES). However, we are not aware of any existing material where this ordered phase ($U > U_c$) honeycomb-lattice calculation would be directly relevant. In the figure, we see that the minimum and maximum gaps are at the W and Γ points, respectively. This dispersion is quite different from the case of the square lattice, since there is no nesting of the Fermi surface here. For the square lattice, the single hole dispersion relation is anomalously flat near the degenerate points $(0, \pm\pi)$, $(\pm\pi, 0)$ of the Brillouin zone, with the minimum of the dispersion at $(\pm\pi/2, \pm\pi/2)$.²³ Figure 10 shows the minimum gap, i.e., the gap at the W point, and the bandwidth,

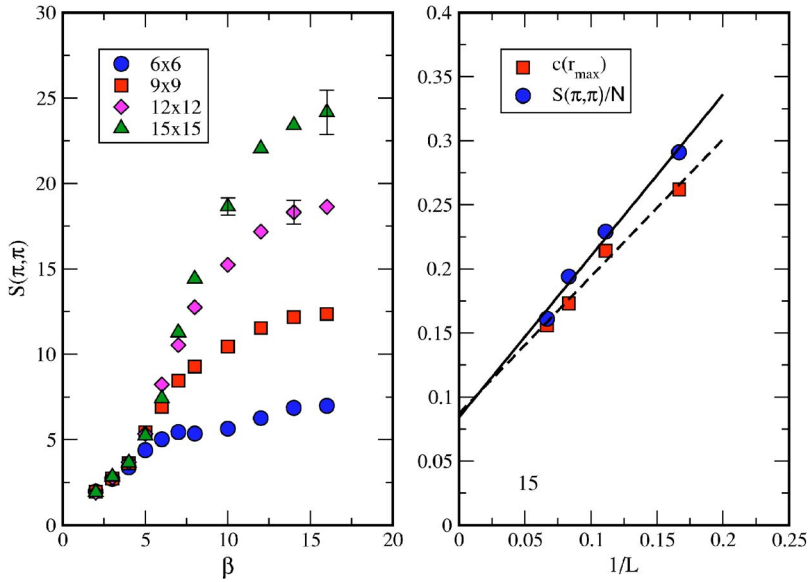


FIG. 5. (Color online) Left panel: the antiferromagnetic structure factor is shown as a function of β and different lattices sizes L at $U/t=7$. At low β (high T) the correlation length is short, and $S(\pi, \pi)$ is independent of L . At large β , $S(\pi, \pi)$ grows with L . Right panel: the scaled structure factor (filled circles) and spin correlation function (filled squares) at large distance are shown for large β as a function of the inverse linear dimension for $U/t=7$. The lines are least squares fits to the data. These quantities scale to a nonzero value of the order parameter (square of the staggered magnetization) in the thermodynamic limit $1/L \rightarrow 0$. Typical error bars are shown on the left panel.

$\Delta_{\Gamma} - \Delta_W$, vs t/U . The gap closes at $t/U \approx 0.26$, indicating a transition to the semimetal phase.

To summarize, study of both magnetic and charge properties using series expansions show a direct transition from the antiferromagnetic to the semimetal phase around $U_c/t \approx 4$.

Combining the quantum Monte Carlo and series expansion results, we estimate the phase transition to be in the range $U_c/t=4-5$. There is greater internal consistency in the location of the critical point if we restrict ourselves to one method. But, in fact, there are larger uncertainties in both methods especially as the quantum phase transition is reached. However, both methods strongly indicate that the Mott transition and the antiferromagnetic order happen simultaneously.

IV. SIGNATURES OF THE QUANTUM PHASE TRANSITION IN THE SPECIFIC HEAT

An important objective of our study was to examine the signature of the quantum phase transition in the finite tem-

perature behavior of the specific heat. We now turn to those studies, which are based on the quantum Monte Carlo method.

At strong couplings, one expects two features in the specific heat of the Hubbard–Hamiltonian. The first, at a temperature $T \approx U/5$, signals the formation of magnetic moments,^{26,27} while the second, at a lower temperature $T \approx J=4t^2/U$, is associated with the entropy of moment ordering. This picture has been verified in the one-dimensional case using Bethe Ansatz techniques²⁸ and (using quantum Monte Carlo) in the two-dimensional square^{29,30} and three dimensional cubic lattices.³¹ Interestingly, in the square lattice, the two peak structure persists to weak coupling where the energy scales U and J have merged.²⁶ In one dimension, there is a single peak at weak coupling.^{32,33}

We have used QMC to calculate the energy as a function of temperature for different couplings U and system sizes. We have used a fine grid of temperatures and then differentiated numerically to extract the specific heat $C(T)=dE/dT$. We have done runs with 4000 sweeps through the lattice and

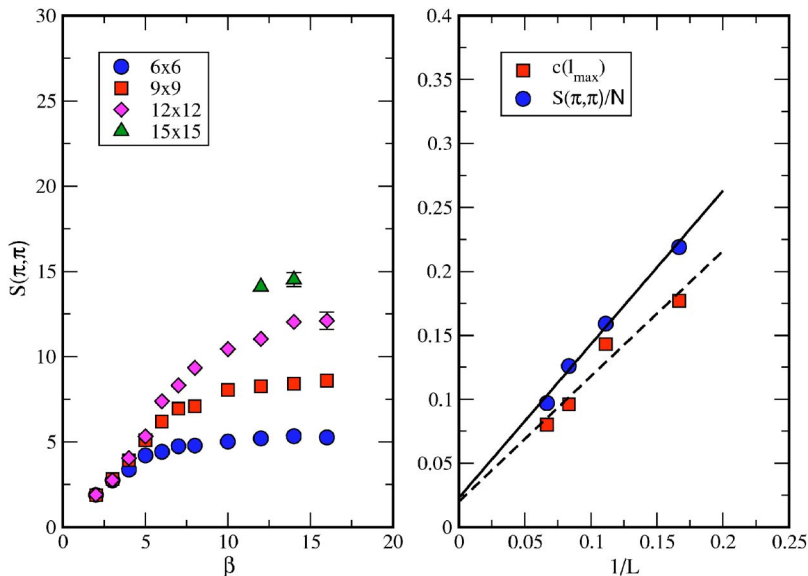


FIG. 6. (Color online) Same as Fig. 5 except $U/t=6$.

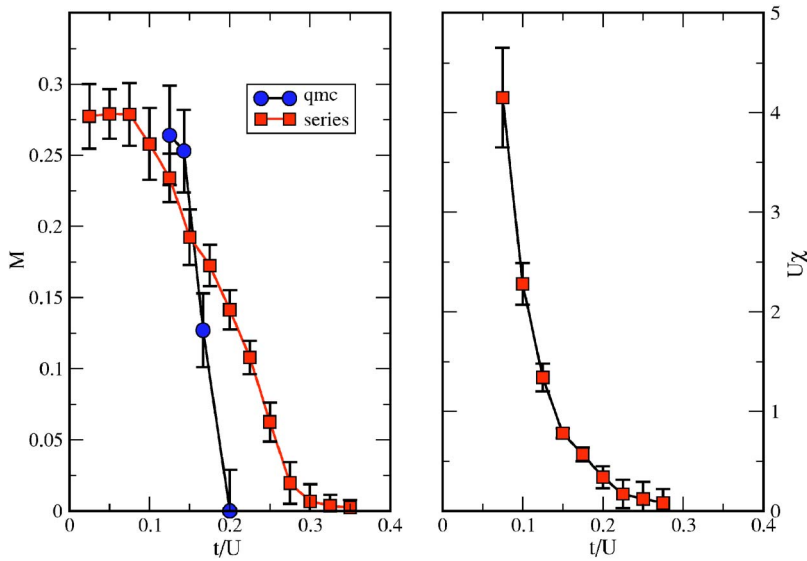


FIG. 7. (Color online) Left panel: the staggered magnetization vs t/U obtained from series expansions and quantum Monte Carlo simulations. The lines joining the points are a guide to the eye. See text for more discussion. Right panel: the uniform susceptibility $U\chi_{\perp}$ vs t/U obtained from series expansion.

for lower temperatures we averaged over several such runs to reduce statistical errors on the energy. For $\beta < 10$ this was enough to ensure that error bars, for a given system size, are smaller than typical data points both in $E(T)$ and $C(T)$. The specific heat for the two-dimensional honeycomb lattice is shown in Fig. 11 for different couplings U and lattice size $L=12$. For strong coupling, $U/t=6, 7, 8$ there is a clear two peak structure. This is replaced by a single peak for weaker couplings, $U/t=2, 4, 5$. Again, this result is in contrast with the behavior of $C(T)$ on the square lattice, where a two-peak structure is evident for all U/t .²⁶ It is plausible to conjecture that the difference is the absence of long range antiferromagnetic order. This suggestion is supported by the fact that coalescence of the specific heat peaks is seen in Dynamical

Mean Field Theory (DMFT)^{34–36} studies when they are restricted to the paramagnetic phase and antiferromagnetic fluctuations are neglected.

This is, however, a rather subtle question, since the Mermin–Wagner theorem precludes long range order at finite temperature, for systems with continuous symmetry in two-dimensions. What is meant, more precisely, is that on a two-dimensional square lattice, the low T structure in $C(T)$ appears when the antiferromagnetic correlation length $\xi(T)$ begins to grow exponentially as $T \rightarrow 0$.

The evolution from a two to a one peak structure in $C(T)$ is one interesting reflection of the underlying quantum phase transition on the finite temperature thermodynamics. Another way of examining this question concerns the low temperature behavior of $C(T)$. As pointed out in the introduction, we expect a quadratic temperature dependence at both strong coupling (spin-waves) and weak coupling (linearly vanishing

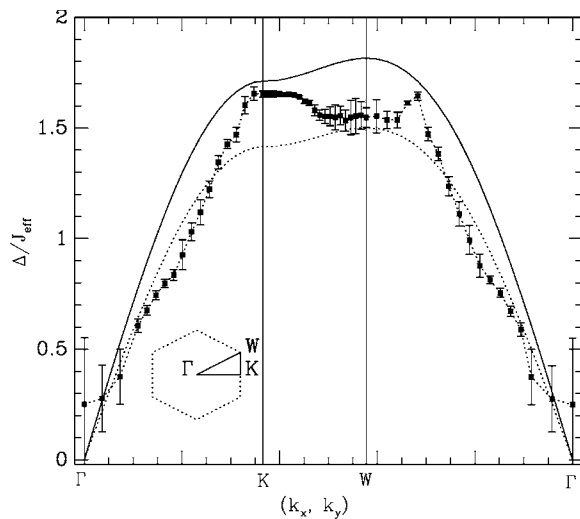


FIG. 8. Plot of the spin-wave excitation spectrum $\Delta(k_x, k_y)$ (in units of effective $J_{\text{eff}}=4t^2/U$) along the path $\Gamma K W \Gamma$ in the Brillouin zone (see the inset, where the momentum \mathbf{k} for Γ, K, W points are $(0,0)$, $(2\pi/3, 0)$, and $(2\pi/3, 2\pi/3\sqrt{3})$, respectively) for the system with coupling ratios $t/U=0.1$ in the Néel ordered phase. Also shown are the first (dashed line) and second (solid line) order spin-wave results (Ref. 22) for Heisenberg model on honeycomb lattice.

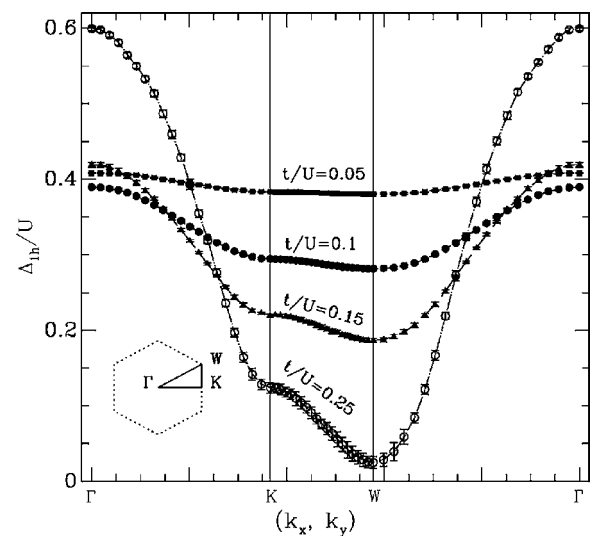


FIG. 9. Plot of the one-hole excitation spectrum $\Delta(k_x, k_y)/U$ in the Néel ordered phase along the path $\Gamma K W \Gamma$ in the Brillouin zone (see the inset) for the system with coupling ratios $t/U=0.05, 0.1, 0.15$, and 0.25 .

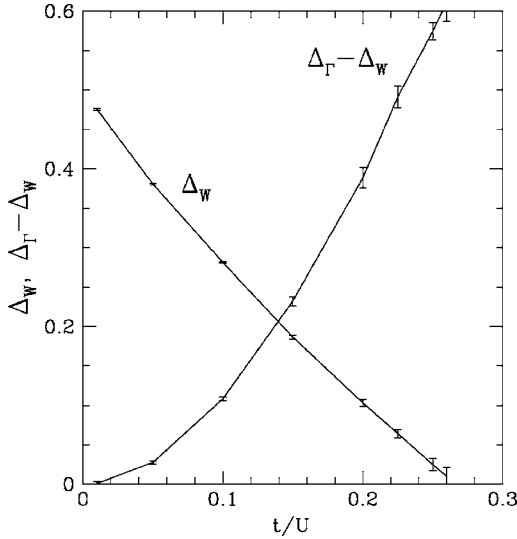


FIG. 10. Minimum single-hole gap Δ_W at W point and its bandwidth $\Delta_\Gamma - \Delta_W$ vs t/U .

density of states at the Fermi level). How does the coefficient δ in $C(T) = \delta T^2$ evolve as one crosses between the two phases?

Before we present the results for δ , we note that extracting δ is clearly a subtle numerical issue. On the one hand, δ characterizes the low T behavior, but on the other hand, because of finite size effects, which become larger as the temperature is lowered, one cannot use data at too low values of T . Thus, our calculation of δ should be viewed with some caution. Finite size effects were probed with the non-interacting system, where they are known to be more severe, and where we could reach larger system sizes. Our procedure to extract δ is as follows: we fit the data for $E(T)$ to the T^3

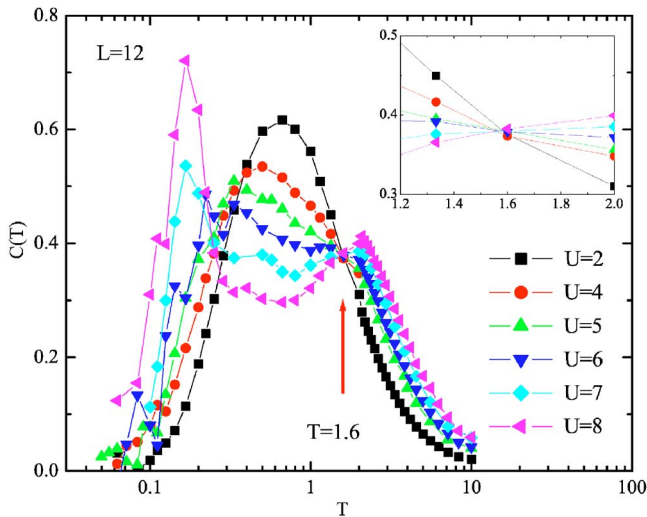


FIG. 11. (Color online) Specific heat $C(T)$ is shown as a function of temperature for different coupling strengths. In the antiferromagnetic phase for $U > U_c$, the specific heat has a two peak structure. In the metallic phase for $U < U_c$ there is a single peak. The “universal crossing” at $T = 1.6t$ is discussed in the text. Error bars (not shown) are typically the size of points for $T > 0.1$, and up to 3–4 times larger for $T \leq 0.1$.

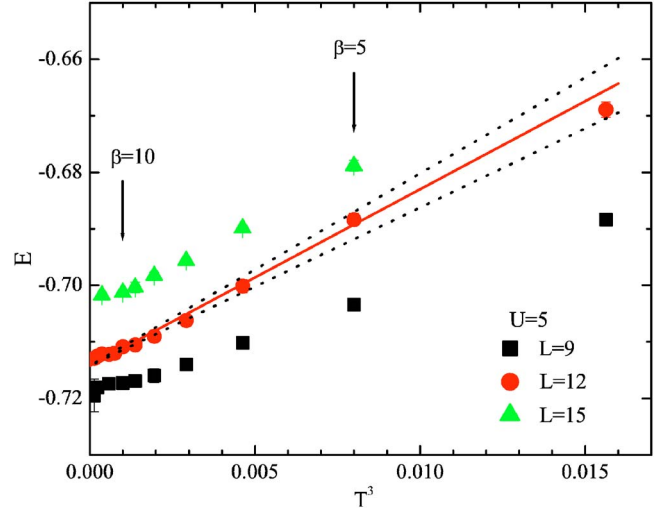


FIG. 12. (Color online) Energy as a function of T^3 for $U/t=5$ and $L=9, 12,$ and 15 . The solid line is the best fit to the data and the dotted lines show the result of a 10% difference in δ . Note that error bars are smaller than points for $5 \leq \beta \leq 10$.

form over only a finite temperature window: below the peak in $C(T)$ but also above finite size effects begin introducing a noticeable gap in spectrum. Figure 12 illustrates this procedure for $U/t=5$, the full line is our best fit to the data. Note that the fit starts to deviate around $\beta/t=5$, where the peak starts to form, but follow the data closely below that. For the noninteracting case the gap becomes noticeable around $\beta/t=10$, therefore for the smaller values of U/t considered, we did not take into account temperatures smaller than $T=0.1t$. This prevented us from getting δ for $U/t < 2$.

In Fig. 13 we show δ as a function of U . There is a structure in this plot in the vicinity of the value $U_c/t \approx 5$ previously inferred from the compressibility and spin correlation data. Fig. 14 emphasizes this feature by plotting the

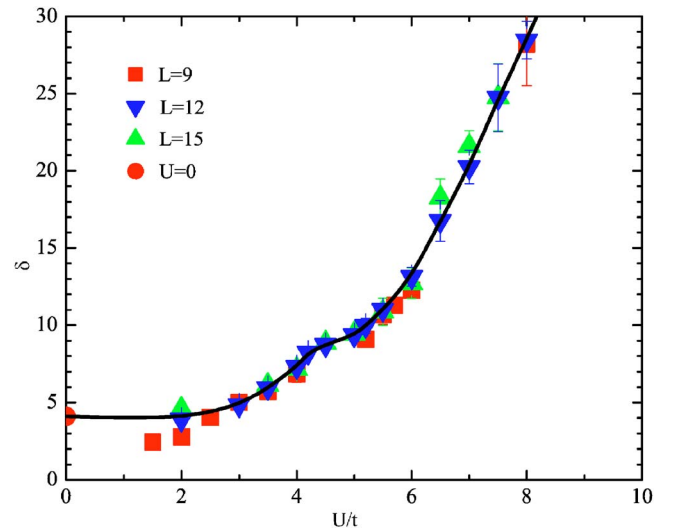


FIG. 13. (Color online) δ , the coefficient of the T^2 term in the specific heat is shown as a function of U/t . The solid square is the $U=0$ value and the line is a guide to the eye. There appears to be a change in slope as U crosses U_c .

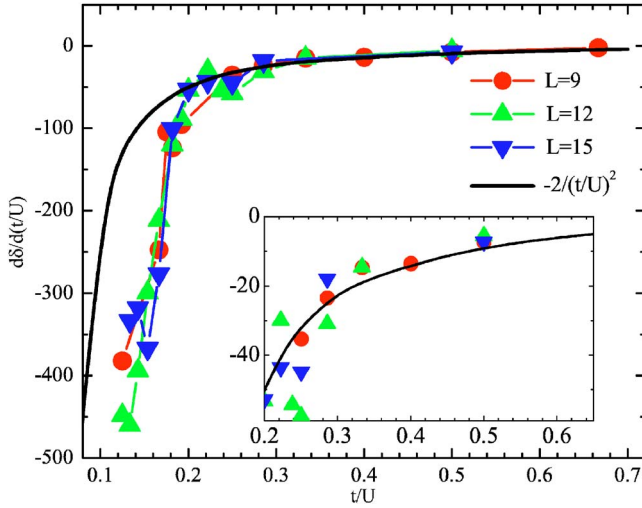


FIG. 14. (Color online) Derivative of δ , the coefficient of the T^2 term in the specific heat, with respect to t/U is shown. This derivative has a sharp change near the critical coupling U_c . The solid line is $-2/(t/U)^2$.

derivative of δ with respect to t/U as a function of t/U . As we have noted, the specific heat of the noninteracting system obeys $C = \delta(U=0)T^2$ with $\delta(U=0) = 4.1$, because of the linearly vanishing density of states. Perturbation theory suggests that for small finite U/t , δ should increase quadratically from this value. Nevertheless, in the vicinity below the quantum phase transition, the value for δ extracted from the quantum Monte Carlo data looks rather linear in U , as seen in Fig. 13. If $\delta = mU/t$ then $d(\delta)/d(t/U) = -m/(t/U)^2$. With this in mind, a line showing the functional form $-m/(t/U)^2$ with $m=2$ is given and fits the weak coupling data very well. The breakaway from this form at strong coupling further emphasizes the change in behavior in the vicinity of the quantum phase transition.

As we have already commented, we found the determination of the specific heat coefficient delta to be challenging. Certainly the data are subject to both possible systematic and statistical uncertainties. Regarding the former, we comment that finite size effects are relatively less profound for local observables like the energy than ones which sample long range correlations (like magnetic structure factors.) We believe that the consistency of the data on $L=9, 12$, and 15 site lattices reflects the fact that the results are representative of the behavior in the thermodynamic limit. We have also checked the effect of the fitting procedure on delta. Figure 12 shows the effect of a ten percent change in delta on the goodness of the fit.

In studies of the two peak structure of the specific heat on the square lattice, an interesting interchange of the role of kinetic and potential energies was noted.²⁶ At large U , the temperature derivative of the potential energy was the primary contribution to the high T , moment formation, peak, while the temperature derivative of the kinetic energy drove the low T , moment ordering, peak. However, at weak U the situation was reversed, with the high T peak originating in the kinetic energy. With that separation in mind, we plot in Fig. 15, for the honeycomb lattice, the contributions of the

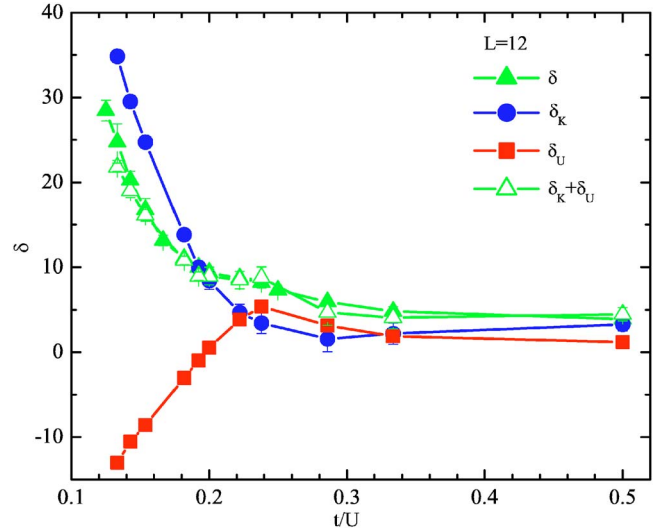


FIG. 15. (Color online) Separate contributions of the potential (δ_U) and kinetic (δ_K) energies to the quadratic coefficient of the specific heat are shown. δ_U shows the more abrupt behavior in the vicinity of U_c . The small differences between the values of δ obtained from the total energy, and the values $\delta_K + \delta_U$ from the kinetic and potential energies separately provide a measure of the uncertainties in our fitting procedure.

potential and kinetic energies to δ . It is the contribution of the potential energy to δ which appears to have the sharper evolution in the vicinity of the quantum phase transition.

Returning to the specific heat versus temperature, shown in Fig. 11, we note the existence of a very well defined crossing point at $T \approx 1.6t$. This crossing has been observed previously in DMFT,³⁴⁻³⁶ and in the two dimensional square lattice.^{26,29} Indeed, in the former case, two crossings were observed, with the high temperature one being nearly universal, while the low temperature intersections were considerably more spread out, much as we observe in Fig. 11. It is also interesting that the numerical value of the crossing is almost identical for the honeycomb and square lattices, despite their different bandwidths.

Finally, we turn to the behavior of the entropy per site S/N . The entropy is calculated from the specific heat:

$$S(T) = \int_0^T \frac{C(T')}{T'} dT'.$$

To do the integral we have fitted the energy to a physically motivated form,

$$E(T) = E_0 + \sum_{n=1}^M c_n e^{-\frac{n\Delta}{T}},$$

where E_0 , Δ and c_n are obtained from the fitting and M is the number of exponentials used, typically 6 to 8. This expression can then be differentiated to get $C(T)$ and then integrated. In the left panel of Fig. 16 we show S/N as a function of U for different temperatures T . For large temperatures the entropy per site approaches $\ln(4)$ for all couplings, indicating that each site can be either empty, singly occupied with spin

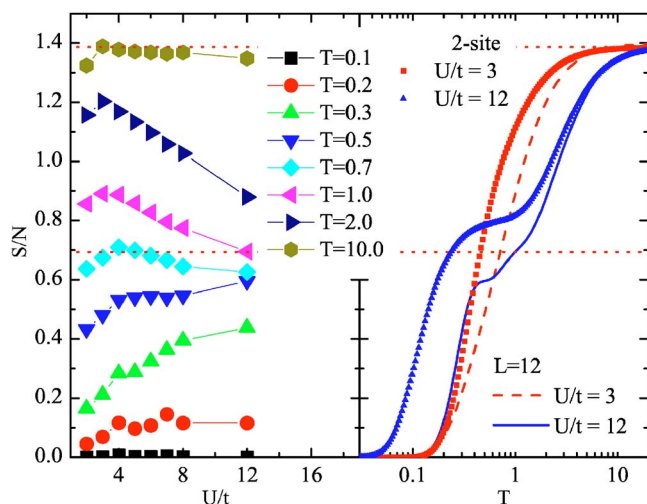


FIG. 16. (Color online) Left panel: the entropy per site is shown as a function of U for different temperatures. At large U the gaps between the $T=10$ and $T=2$ curves and between the $T=0.3$ and $T=0.2$ curves reflect the entropy loss associated with magnetic moment formation and ordering, respectively. Right panel: the entropy per site is shown as a function of T for weak and strong coupling. The dashed and solid lines are the results of quantum Monte Carlo simulations on 12×12 lattices. The squares and triangles are generated by an exact calculation on a two site model for comparison.

up, singly occupied with spin down or doubly occupied with the same probability. At large U , the clustering of the curves for different temperatures near $\ln(2)$ is indicative of the existence of disordered magnetic moments (only singly occupied states) in a range of intermediate T . The low temperature magnetic ordering tendency is evident in the gap between the $T=0.2$ and $T=0.3$ curves. As U is decreased, the screening away of the moments is indicated by the $T=0.3$ isotherm dropping from $\ln(2)$ to 0. It is interesting that this behavior is so gradual. Finally at small U one observes the more or less equally spaced isotherms of free electron gas. This figure complements the data of $C(T)$ shown in Fig. 11, since the entropy hang up at large U near $\ln(2)$ is just the C/T area of the lower specific heat peak.

The right panel of Fig. 16 exhibits the entropy as a function of temperature. At weak coupling, there is a smooth evolution from $\ln(4)$ at high T to zero at low T . For strong coupling, a plateau near $\ln(2)$ interrupts this evolution, again exhibiting a range of temperatures with well formed, but disordered moments.

V. CONCLUSIONS

In this paper we have studied the Hubbard–Hamiltonian on a half-filled honeycomb lattice using quantum Monte

Carlo and series expansion methods. Both methods strongly suggest that the model has a single continuous transition at $T=0$, between an antiferromagnetic phase at large U/t and a semimetal phase at small U/t . Quantum Monte Carlo results for the compressibility, which looks at the charge response of the system, and the magnetic structure factor, which looks at the spin response, both suggest a transition around $U_c/t \approx 5$. The series expansion results for the sublattice magnetization, which is the spin order parameter and the charge excitation gap, which characterizes the Mott transition, both point to a single transition at $U_c/t \approx 4$. The discrepancy between the quantum Monte Carlo and series expansion results reflects the uncertainties in the calculations, especially as the critical point is approached. Thus we expect the transition to lie in the range $4 < U_c/t < 5$, a result in complete agreement with the previous work of Martelo *et al.*⁴

Finally, one of the goals of this work was to look for finite temperature signatures of the phase transition in the specific heat, as a guide to experimental studies. We observe that around U_c the specific heat changes from a one peak (below U_c) to a two peak (above U_c) structure. We suggest that this is associated with the fact that for $U > U_c$ the antiferromagnetic correlation length grows rapidly as the temperature is reduced. For weak coupling only very short-range antiferromagnetic correlations exist, and the specific heat has no signature of magnetic order.

We also studied the evolution with on-site interaction strength U of the coefficient $\delta(U)$ of the quadratic temperature dependence of the specific heat at low temperatures. Since the excitations which produce the T^2 term above and below the quantum phase transition are unrelated, one might have expected $\delta(U)$ to exhibit a discontinuity at U_c . Instead, we found a sharp change in the slope, $d\delta(U)/dU$ at U_c . Given the uncertainties in obtaining $\delta(U)$, from finite-size calculations, these results should be viewed with some caution. Experimental searches for such a behavior would be quite interesting.

ACKNOWLEDGMENTS

We acknowledge very useful conversations with W.E. Pickett and A.K. McMahan. This work was supported by the CNPq-Brazil, FAPERJ-Brazil and FUJB-Brazil (TP), U.S. National Science Foundation Grants Nos. DMR-0312261 (RTS), INT-0203837 (RTS), and DMR-0240918 (RRPS), and by a grant from the Australian Research Council (W.Z. and J.O.). W.Z. wishes to thank the University of California at Davis for hospitality while part of the work was being done. We are grateful for the computing resources provided by the Australian Centre for Advanced Computing and Communications (AC3) and by the Australian Partnership for Advanced Computing (APAC) National Facility.

- ¹See, *The Hubbard Model*, edited by A. Montorsi (World Scientific, Singapore, 1992); *The Hubbard Model-Recent Results*, edited by M. Rasetti (World Scientific, Singapore, 1991); and references therein.
- ²D. J. Scalapino, in *Does the Hubbard Model have the Right Stuff?* edited by R. A. Broglia and J. R. Schrieffer, *Proceedings of the International School of Physics, Enrico Fermi, Course CXXI* (North-Holland, Amsterdam, 1994).
- ³S. Sachdev, in *Quantum Phase Transitions* (Cambridge University Press, Cambridge, UK, 1999); S. L. Sondhi, S. M. Girvin, J. P. Carini, and D. Shahar, *Rev. Mod. Phys.* **69**, 315 (1997).
- ⁴L. M. Martelo, M. Dzierzawa, L. Siffert, and D. Baeriswyl, *Z. Phys. B: Condens. Matter* **103**, 335 (1997).
- ⁵S. Sorella and E. Tosatti, *Europhys. Lett.* **19**, 699 (1992).
- ⁶N. Furukawa, *J. Phys. Soc. Jpn.* **70**, 1483 (2001).
- ⁷N. M. R. Peres, M. A. N. Araujo, and D. Bozi, *cond-mat/0403605*.
- ⁸T. Hanisch, B. Kleine, A. Ritzl, and E. Müller-Hartmann, *Ann. Phys.* **4**, 303 (1995).
- ⁹G. Baskaran and S. A. Jafari, *Phys. Rev. Lett.* **89**, 016402 (2002).
- ¹⁰J. González, F. Guinea, and M. H. Vozmediano, *Nucl. Phys. B* **424**, 595 (1994).
- ¹¹L. Balents and M. P. A. Fisher, *Phys. Rev. B* **55**, R11973 (1997).
- ¹²<http://cst-www.nrl.navy.mil/hellberg/projects/csh.html>
- ¹³See, for example, W. Zheng, J. Oitmaa, C. J. Hamer and R. R. P. Singh, *cond-mat/0403718*.
- ¹⁴R. Blankenbecler, D. J. Scalapino and R. L. Sugar, *Phys. Rev. D* **24**, 2278 (1981).
- ¹⁵R. T. Scalettar, D. J. Scalapino, R. L. Sugar, and D. Toussaint, *Phys. Rev. B* **36**, 8632 (1987); S. R. White, D. J. Scalapino, R. L. Sugar, E. Y. Loh, J. E. Gubernatis, and R. T. Scalettar, *ibid.* **40**, 506 (1989).
- ¹⁶J. E. Hirsch, *Phys. Rev. B* **31**, 4403 (1985).
- ¹⁷R. T. Scalettar, R. M. Noack, and R. R. P. Singh, *Phys. Rev. B* **44**, 10502 (1991).
- ¹⁸M. P. Gelfand and R. R. P. Singh, *Adv. Phys.* **49**, 93 (2000).
- ¹⁹Z. P. Shi and R. R. P. Singh, *Phys. Rev. B* **52**, 9620 (1995).
- ²⁰M. P. Gelfand, *Solid State Commun.* **98**, 11 (1996).
- ²¹C. J. Hamer, W. Zheng and R. R. P. Singh, *Phys. Rev. B* **68**, 214408 (2003).
- ²²W. Zheng, J. Oitmaa, and C. J. Hamer, *Phys. Rev. B* **44**, 11869 (1991).
- ²³See, for example, C. J. Hamer, Z. Weihong, and J. Oitmaa, *Phys. Rev. B* **58**, 15508 (1998).
- ²⁴D. A. Huse, *Phys. Rev. B* **37**, 2380 (1988).
- ²⁵A. J. Guttmann, in *Phase Transitions and Critical Phenomena*, edited by C. Domb and J. Lebowitz (Academic, New York, 1989), Vol. 13.
- ²⁶T. Paiva, R. T. Scalettar, C. Huscroft, and A. K. McMahan, *Phys. Rev. B* **63**, 125116 (2001).
- ²⁷See also Fig. 36 in A. Georges *et al.* *Rev. Mod. Phys.* **68**, 13 (1996).
- ²⁸M. Takahashi, *Prog. Theor. Phys.* **52**, 103 (1974).
- ²⁹D. Duffy and A. Moreo, *Phys. Rev. B* **55**, 12918 (1997).
- ³⁰R. Staudt, M. Dzierzawa, and A. Muramatsu, *Eur. Phys. J. B* **17**, 411 (2000).
- ³¹R. T. Scalettar, D. J. Scalapino, R. L. Sugar, and D. Toussaint, *Phys. Rev. B* **39**, 4711 (1989).
- ³²H. Shiba and P. A. Pincus, *Phys. Rev. B* **5**, 1966 (1972).
- ³³J. Schulte and M. C. Böhm, *Phys. Rev. B* **53**, 15385 (1996).
- ³⁴A. Georges and W. Krauth, *Phys. Rev. B* **48**, 7167 (1993).
- ³⁵D. Vollhardt, *Phys. Rev. Lett.* **78**, 1307 (1997).
- ³⁶N. Chandra, M. Kollar, and D. Vollhardt, *Phys. Rev. B* **59**, 10541 (1999).